[C_{II}] line emission at the epoch of reionisation

Marc Van den Bossche[1,2], supervised by Laura Keating[2], and Norman Murray[2]

[1] *Département de Physique, École Normale Supérieure, 75005, Paris, France*
[2] *Canadian Institute for Theoretical Astrophysics, University of Toronto, ON, M5S 3H8, Canada*

Internship report
from February, 12th to July, 15th 2019

Abstract

In this report I present the results of attempts at simulating [C_{II}] line emission images of individual high-redshift galaxies. This is motivated by the observation of larger than expected [C_{II}] halos at redshift 5 to 7 by Fujimoto *et al.* in early 2019. First I present the techniques needed to go from zoom-in cosmological galaxies simulations to [C_{II}] line emission. Then I confirm that the halos I am studying are comparable to observed galaxies at those redshifts. Finally I compare my results with observation and try to discriminate scenarios proposed by Fujimoto *et al.* to explain larger [C_{II}] emission halos. The most likely scenario is violent feedback effect such as supernoæ at this point.

You just come along with me and have a good time. The Galaxy's a fun place. You'll need to have this fish in your ear.
—Douglas Adams, The Hitchhicker's Guide to the Galaxy

Contents

Introduction

The first galaxies and stars of the universe are thought to have formed during the first billion years after the big bang (redshift 1100 to 6), this is called the epoch of reionisation [Fan et al., 2006,McGreer et al., 2011]. Yet there still is a lot to learn about the exact formation of structures like galaxies. The first theories, which have now been ruled out, had a top-down approach. It was thought that galaxies formed as huge gas clouds that collapsed to form a disk. The stars would then later form when the cooled gas is no longer gravitationally stable [Eggen et al., 1962]. The more recent theory have the opposite idea. First small clumps of stars formed and they later merged into galaxies [White and Rees, 1978]. Most of those galaxies then coalesce into protocluster (at about one billion years after the big bang), then into galaxy clusters (around three billion years after the big bang) and then into superclusters (around five billion years after the big bang). Even though we now have a better insight on the general galaxy formation process, we do not completely understand its details yet.

Studying galaxies, be it with simulation, analytic computation or observation is hence strongly motivated by the will to understand the early history of our universe and to find a cosmological model consistent with observations.

Simulating galaxies is a convenient tool. It allows us to test theories and also to interpret observations. There are however a large choice of galaxy simulation types, depending on the exact subject of interest. Here I will use the FIRE[1] simulations [Hopkins et al., 2014], best know for their feedback feature. The simplest way to study a galaxy is to study the light coming from it. The most obvious light source are the stars of the galaxy, as in most galaxies they are the brightest sources. Yet there also is a lot of interstellar medium gas that emits light which we can study.

Individual galaxies at high redshift

In this work I focus on galaxies at redshift 5 to 7. These are the first galaxies that formed in the universe. Being able to reproduce their properties with simulations starting at early universe initial conditions [Hahn and Abel, 2011] is a way to probe that the physics leading to galaxy formation is understood.

Even though line-intensity observations can be challenging, because lines can be very dim when looking at high-redshift galaxies, it is a very useful technique. As reported in [Kovetz et al., 2017], this technique has now been stretched to many molecular, atomic and ionic lines. If one looks at one specific emission line with a finite thermal width, using a good enough resolution, one can examine the velocity structure of a molecular cloud or a galaxy, taking advantage of the Doppler-shift. This is a key asset of this technique. The line emission of well-known molecules can also be used to determine the local properties of the interstellar gas like its temperature and density along different lines of sight. With the advent of new telescopes and in particular ALMA[2], it has become possible to look at individual galaxies at high redshift with the [C_{II}] 158μm-line[3]. An other bright and commonly-used line is the J=1 to J=0 line of carbon monoxide. [C_{II}] and CO-line are the brightest lines of the interstellar medium, here we will focus on the [C_{II}] line only. For example the velocity structure [Dayal and Ferrara, 2018, Kohandel et al., 2019, Smit et al., 2018] and more general properties [De Looze et al., 2011] of such galaxies are being mapped and studied. An example of high-redshift [C_{II}]-line galaxy observation is shown on figure 1.

The FIRE simulation

The FIRE simulations are nowadays part of the best resolution large scale cosmological simulations. There are several reasons for that. The first version of the code, which produced the first set of simulations "FIRE

[1] Feedback In Realistic Environments – One of the main strengths of these simulations is feedback phenomena, we will discuss this in more details later.

[2] Atacama Large Millimeter/submillimeter Array in Chile. The first paper using data from this telescope was published in 2012 [de Ugarte Postigo, A. et al., 2012].

[3] This line, noted [C_{II}], corresponds to the transition from the only excited state of C_{II} to its fundamental state.

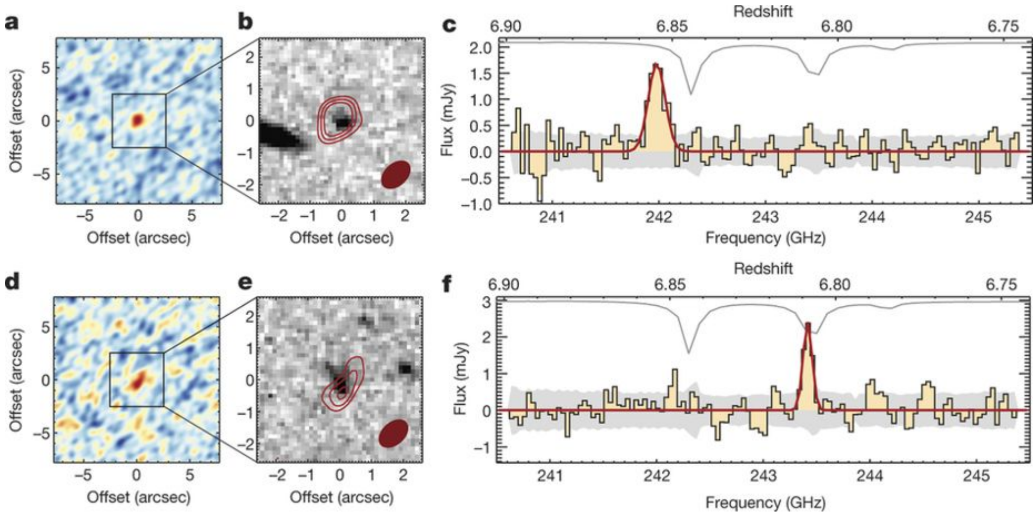

Figure 1: Example of redshift 6.8 galaxy image looking at the [C_{II}] line with ALMA. Velocity fields measured in galaxies COS-3018555981 (a-b-c) and COS-2987030247 (d-e-f), two Lyman-break galaxies. The ellipse on the bottom-right of picture (b) and (e) shows the size of the ALMA beam. The highest peak on (c) and (f) is the [C_{II}] line of those galaxies. Figure 1 from [Smit et al., 2018].

1" [Hopkins et al., 2014], already included a lot of physics relevant to large-scale cosmological phenomena and the code has recently been improved, and now combines even more physical phenomena. In this work I used simulations done with the latest, improved and more comprehensive version of the code: "FIRE 2" simulations [Hopkins et al., 2018a]. In this report I will focus on the physics included in this version (which will be refereed to simply as "FIRE" from now on).

The two basis elements of the FIRE set-up are a meshless finite-mass hydrodynamic solver and an N-body gravitation solver (both solvers are combined in a code called GIZMO[4], an improved GADGET-3 for the N-body solver part.) [Hopkins, 2015]. In order to have relevant results for a cosmological large-scale simulation, more physics than those two basic elements needs to be included. The other strengths of the FIRE set-up is that it also includes a gas-cooling algorithm as well as a star formation algorithm. The main asset of the FIRE set-up is that it also includes a realistic implementation of stellar feedback. Feedback means taking into account the impact of formed stars on their environment beyond photo-heating (stellar winds, supernovæ ...). This enables to achieve simulations closer to the actual observations than what previous large-scale cosmological simulations did. Aside from its better resolution than previous simulation set-ups, it is also possible to add a lot of additional physics to the "core" FIRE code. For example, one can add magnetic fields, conduction, viscosity, diffusion, cosmic rays, black holes, and more...

As reported in [Hopkins et al., 2018a], the FIRE simulation has been successful in more than just one facet of large-scale cosmological simulation. It is indeed one of the highest resolution simulation set if one wishes to look at individual galaxies in a fully cosmological context. The feedback phenomena that were implemented in the code now render the simulation set comparable with observation thanks to physically motivated prescriptions for star formation and their feedback effects. The GIZMO code also explicitly follows a multiphase interstellar medium, *i.e.* a wide portion of the relevant temperature-density phase space. Thanks to these, one can use the FIRE simulation to study galaxies in a wide range of redshift. On figure 2 one can see a mock Milky Way-like galaxy at redshift 0 rendered by FIRE. Such galaxies can be compared to local galaxies in hope to better understand physics that telescope are not yet resolving.

Motivation

Using large-scale cosmological simulations is a good way to probe cosmological models and check that the basic cosmological principles that current cosmology and astrophysics assume indeed match the real universe [Planck Collaboration, 2016]. For example, one can look at galaxies from the epoch of reionisation. Some of them, namely the ones that were first observed with the Lyman-α line, do not match the local scaling relations in term of [C_{II}] luminosity [Ouchi et al., 2013, Ota et al., 2014, Maiolino et al., 2015, Knudsen et al., 2016, Pentericci et al., 2016]. Comparing simulation data to observation for those galaxies can help us find the physics that we miss with the local scaling relationships. One can also use simulation as a tool to look at interstellar and intergalactic medium as well as circum galactic medium (around - but not inside - the galaxy) that are usually

[4]This is not an acronym, this name was chosen as a reference to the GADGET code, with which GIZMO shares a lot of code.

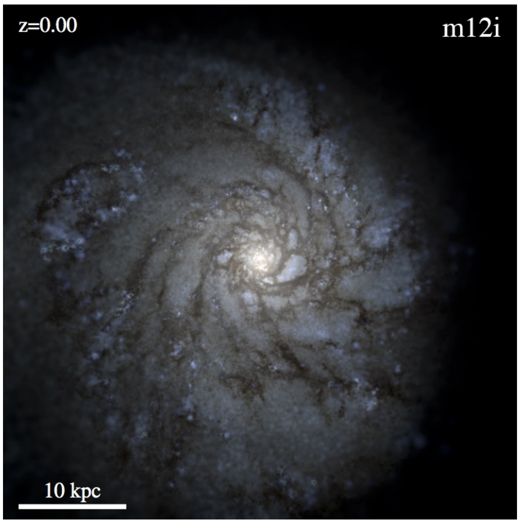

(a) Top view.

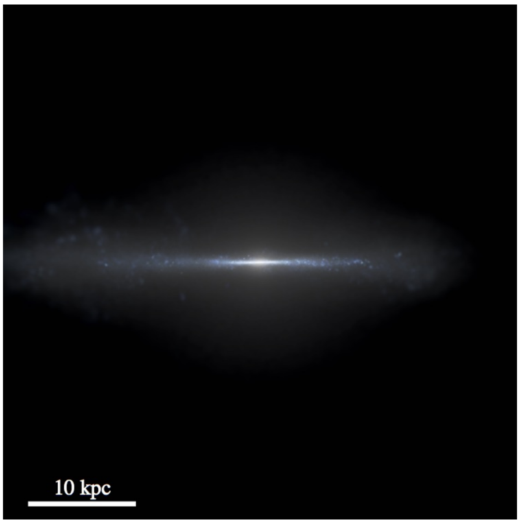

(b) Edge-on view.

Figure 2: Mock images of a Milky Way-mass galaxy at redshift 0 simulated with FIRE-2 (images taken from [Hopkins et al., 2018a]). Those images are rendered following the method described in [Hopkins et al., 2005] to mock Hubble Space Telescope images.

more difficult to study as they are not as luminous than the stars and dust in a galaxy.

Observations of [C_{II}] halos

A recent study of ALMA observations has shown the existence of a larger than expected [C_{II}] halo in galaxies at redshift between 5 and 7 [Fujimoto et al., 2019]. That paper reports that the [C_{II}]-line light comes from a region of 10 kiloparsec radius. They obtained this result stacking 18 galaxies to reduce noise level (these observations are reported on figure 3 of this report). They chose these galaxies have certain properties. For instance they selected them (i) to have a stellar formation rate lower than 100 $M_\odot$/yr, (ii) not to show sign of AGN[5] activity. (iii) The galaxies also are not to be giant Lyman-α systems[6], (iv) not to show signs of gravitational lensing, (v) such that the line width of the [C_{II}] is wider than 80 km/s (Doppler-shift) and (vi) that they reproduce the [C_{II}] line emission in their own data reduction. Such a [C_{II}] halo scale is unexpected because the rest-frame UV emitting region that they also observed with ALMA is smaller (according to Fujimoto *et al.* it has a radius of 7 kpc).
In this paper they try to reproduce their observations with their star forming simulation, Althæa [Pallottini et al., 2016, Pallottini et al., 2017, Behrens et al., 2018]. They report that their simulation fails to reproduce a 10 kpc scale [C_{II}] halo. However they propose five scenarios that could explain why there is such a spatial extension for [C_{II}] emission in those galaxies. Those scenarios are the following ones.

a) There are satellite galaxies near the observed halos but are not resolved. There is [C_{II}] emission on a larger scale because the gas "belongs" to those sub halos.

b) There is a photo-dissociation region spanning over circum-galactic scales (CG-PDR). No physical motivation is provided by Fujimoto *et al.* for this scenario.

c) Similarly to the previous scenario, there could be photo-ionisation on a circum-galactic scale. The Lyman-α emission region would also be larger with this scenario. Be it stars on a larger scale or UV-thin gas in the disk, there are ionising photons on a larger scale.

d) There could be cold stream of matter as can be seen for star forming galaxies at those redshift in simulations [Dekel et al., 2009].

e) Finally there could also be outflows of gas from the halos. Outflow can be a consequence of stellar formation feedback, for instance supernovæ or stellar winds.

[5] Active Galactic Nucleus – a compact region in the galactic disk that produces much brighter light than normal in at least one part on the electromagnetic spectrum with indication that the light is not produced by stars.
[6] Like for example Himiko [Ouchi et al., 2009] or CR7 [Matthee et al., 2015].

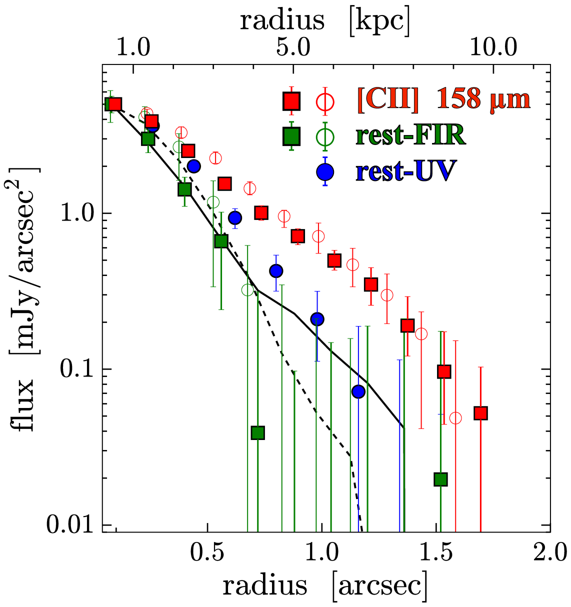

Figure 3: This is the observed data presented in [Fujimoto et al., 2019]. It shows the flux of [C_{II}] emission obtained by stacking 18 observed galaxies as a function of galactic radius. The red squares correspond to the [C_{II}] line emission, the green squares to the rest-frame far-infrared (FIR) and the blue cirlces correspond to the rest-frame ultra-violet emission. The FIR emission correspond to the dust continuum emission in the galaxies and the UV emission correspond to the light emitted by the stars of the halos. This is figure 6 from [Fujimoto et al., 2019].

It is also possible that more than one scenario is what actually happens, be it for different halos, or even several of them happening at the same time in one given halo.

In the present work I have tried to reproduce a similar [C_{II}] halo scale in the FIRE simulations. I will be using FIRE runs at redshift between 5 and 7 like reported in the observation paper. This simulation set is described by X. Ma [Ma et al., 2018b, Ma et al., 2018a]. I will then see whether one or more of the scenarios proposed by Fujimoto *et al.* can be excluded or confirmed with the FIRE simulations.

In a first part I introduce the numerical methods that I used, ranging from the FIRE simulations to the post processing steps that I went through in order to produce observation mocks of ALMA observations. Then in chapter two, I present general properties of FIRE galaxies at redshift between 5 and 7, and properties of the interstellar medium of those galaxies. In chapter three I show preliminary [C_{II}] emission results. I also examine the spatial extension of the [C_{II}] halo and propose a more detailed explanation for the large [C_{II}] scale, further precising the scenarios presented by Fujimoto *et al.* [Fujimoto et al., 2019].

Chapter 1

Numerical methods

One has access to much more local data when using simulation than when using observational data. Here we know exactly the position of each gas cell as well as its density and local temperature. However in order to render line intensity maps we have to go through different steps. First we will quickly look at the general processes at work in the FIRE simulation set-up and look at the physics they describe. Then we will examine the chemistry in the CHIMES programme I used to compute the abundances of molecules in the gas cells. Then one has to compute the radiative transfer of the gas cell for the atomic or molecular lines of interest. To do so I used the RADMC-3D programme, the physics of which I will discuss in a third part.

1 The FIRE simulation set-up

The FIRE simulation set-up is the combination of a hydrodynamics and an N-body solver for gravity. Yet in order to have realistic outputs, one has to incorporate more physics to it. To this solver are added heating and cooling processes, star formation processes, in a multi-phase interstellar medium. The main strength of the FIRE code is that it uses so called feedback phenomena. Using feedback is not a new idea, but in FIRE it is how it has been implemented that is different from what has been done previously. We will quickly examine every physical process that has been included in the "core" FIRE set-up.

1.1 Physics in the FIRE simulation

Hydrodynamics solver First let us take a look at the implemented hydrodynamics solver GIZMO [Hopkins, 2015]. The usual methods used to solve multi-dimensional hydrodynamics problems are SPH (Smoothed-Particle Hydrodynamics) and Mesh methods (Unstructured, moving, etc). Both these methods have advantages, but they also suffer from important drawbacks. For instance SPH methods are known to have difficulties with sharp-shocks, fluid mixing instabilities and anisotropic diffusion, amongst other phenomena. For this reason, meshless methods have been implemented in GIZMO.

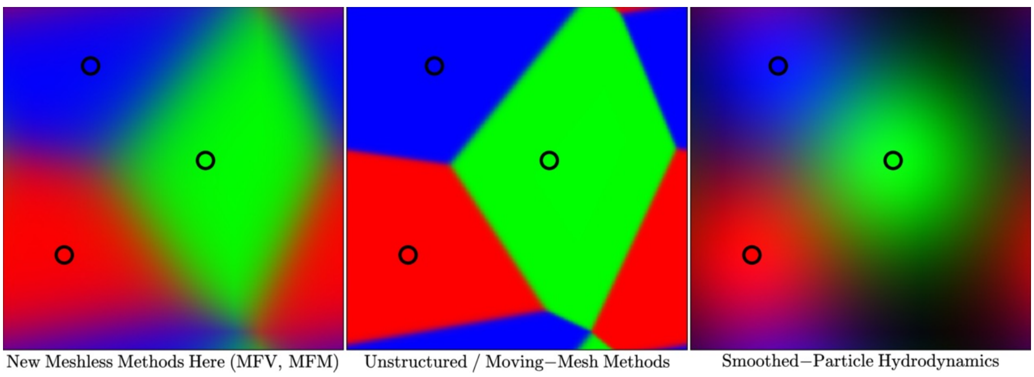

Figure 1.1: This figure represents the differences between the meshless methods, the mesh methods and the SPH methods in a visual way. **Left:** For the meshless finite-volume or meshless finite-mass methods, the volume partition is given by a smooth kernel decomposition at each point. Even though the kernel functions are spherical, the domain associated to each particle is not. **Centre:** For the mesh methods, the boundaries are strict. Note that this is exactly the limit of the MFM/MFV method for an infinitely sharply-peaked kernel function. **Right:** This is the SPH volume partition. The equations of motion are evaluated at each kernel (black circles) using weighted averages from the volume partition function. Figure from [Hopkins, 2015].

When one runs GIZMO it is possible to choose which hydrodynamics solver one would like to use. The usual Cartesian Fixed-Grid, SPH, Moving Voronoi Meshes methods are implemented as well, but let us quickly review the meshless methods that were developed for those simulations. The Meshless Finite-Volume (MFV) method uses kernel functions to partition the volume but in an exact analytic way, unlike SPH. The equations define an effective face for the particles and an exactly conservative Riemann problem is solved there. This method captures sharp discontinuities more accurately than the other methods listed above. The mass of the fluid particle evolves according to the dynamics at its faces. The second meshless method available is the Lagrangian Meshless Finite-Mass (MFM) method. This methods is very similar to MVM but one assumes a deformation of the faces of the particles such that there is no mass flux between particles. A visual demonstration of these new methods compared to usual ones is presented on figure 1.1.

Heating and cooling Then we will inspect the simple heating and cooling processes that are included in the FIRE set-up. In FIRE simulations, a lot of information is attached to each gas particle. Their metallicity is one of the quantities one can follow through the simulation. It is the mass fraction of elements with higher atomic number than Helium. The FIRE simulation follows the mass fraction of eleven elements. However it does not look at the possible chemical reactions that can occur between them. The code uses those abundances to compute the cooling rate of the gas cell using pre-tabulated rates depending on the gas density, metallicity and temperature.
Heating in the FIRE simulations comes from star heating the gas and dust around them with radiative heating. The second source of heating is shock heating, that happens when the gas is violently pushed from where it was by some feedback phenomenon. The heating processes also include photo-heating from an extra-galactic UV background.
The cooling mechanism includes cooling processes like free-free, photo-ionisation/recombination, Compton, photo-electric, metal-line, molecular, fine-structure, dust collisional, and cosmic ray. The range of temperature that the code handles for the gas cells is from 10 K to 10^{10} K [Hopkins et al., 2018a].

Star formation The star formation process is included for all the gas cells of the simulation box. Once they reach certain conditions the code will initiate the star-forming algorithm. The conditions for the star formation to happen are the following ones. The gravitation potential created by the gas cell has to be larger than the thermal energy of the cell together with its kinetic energy, within the resolution scale. The self-shielded gas fraction has to be above a threshold fraction. The thermal Jeans mass of the cell has to be below the mass of the cell, this is a criterion telling us that the gas in the cell will gravitationally collapse. The last condition upon which the star formation process will begin is that the gas cell has to reach a critical density. This star formation process correspond to the collapse of the gas in the cell into stars.

Feedback processes As we already discussed adding feedback processes to a large scale cosmological hydrodynamics simulations has been done before FIRE (FIRE 1 and FIRE 2) [Katz, 1992], but the code used for this simulation pays particular attention to it. The feedback includes several mechanisms. The first one is supernovæ types Ia and II that blow the gas away from where they happen with great velocity. An other process is the continuous stellar mass-loss due to stellar winds. The code also includes Photo-ionisation and photoelectric heating feedback where each star cell is treated as a source with appropriate age, metallicity-dependent spectrum. The last feedback process included to the GIZMO code is radiation pressure. Each tracked photon transfers its momentum upon absorption.

The result obtained after one added those feedback processes was that the star formation rate in halos dropped to match the rates inferred from observations. Before adding them the FIRE halos usually had more stars that what is actually observed. Afterwards the stellar mass of halos also matched the one derived from observational data and previous analytic studies [Shetty and Ostriker, 2008, Kim et al., 2011, Hopkins et al., 2018b, Faucher-Giguère et al., 2013, Quataert et al., 2011, Hopkins et al., 2012].

1.2 Discretisation in FIRE

As with every simulation the discretisation plays an important role and if one does not pay enough attention to it, it can sometimes lead to non-physical effects. In this subsection, I will only present the basics of the discretisation used in FIRE. We will first examine particle types of the code and then we will take a look at the resolution of the simulation for those particle types.

Grids and particle types The hydrodynamics solver part of the FIRE code take more than just one field into account. There are two dark matter fields (one with better resolution than the other), a star field and a gas field [Hopkins et al., 2018a]. The dark matter fields have a coarser resolution than gas by about a factor

five in mass. The star field as well as the dark matter field are considered collisionless. The reason why there are two dark matter field and a gas (matter) field is that we wish to model a realistic cosmological environment for the halo (or few halos) of interest. Yet having fine resolved matter and dark matter cells everywhere in the simulation box, which is ten to hundreds megaparsec wide, would be very computationally expensive. Doing so with different resolution for different field is the happy middle in between, sufficient resolution to be able to look at the galactic interstellar medium and to have a realistic halo environment.
In the star formation process discussed in the previous subsection, we saw that gas cells turn into star cells. This is done in such a way that the cell mass stays approximately the same before and after the transformation. We also mentioned that the star cell loose mass because of star wind and supernovæ this means that all particles will not have exactly the same mass. However in the FIRE code is included a feature that ensures that the gas particles roughly have the same mass. Particles with too low a mass will merge and too heavy particles will split.

Resolution Like most hydrodynamics code, the GIZMO part of FIRE has a well defined mass-resolution. The resolution mass for FIRE range from 56×10^3 $M_\odot$ [Hopkins et al., 2018a] up to 250 $M_\odot$ [Hopkins et al., 2018a][1] on the highest resolution runs. In order to resolve all relevant physical phenomena, the resolution has to big good enough. The most resolution-demanding phenomena are the interstellar medium properties, the star formation and the stellar feedback. Here I used runs with a 7100 $M_\odot$ resolution. I used this resolution because those runs were the runs with the best resolution available for massive halos at those redshift($\simeq 10^{12}$ $M_\odot$ halos[2]).

In order to capture in a reliable way the star formation process, it has been shown (references in 4.1.3(i) of [Hopkins et al., 2018a]) that one shall resolve the existence and self-gravity of the largest self-gravitating gas structure in a galaxy disk.
One shall also take into account the conversion of energy into momentum in unresolved Sedov-Taylor phases due to supernovæİn other words, one shall have small enough cells such that there is enough time between each supernova event for the interstellar medium to cool.
An other non-physical effect that can arise at a low enough resolution is that dwarf galaxies might be more "bursty" than what they should. This is due to the fact that most of the stars of the galaxy will be in only a few star cell and supernova events will have a much more dramatic effect because supernovæ would then be more clustered than they are in reality.
As pointed out by Hopkins *et al.* in [Hopkins et al., 2018a] it is a misconception to think that one needs to resolve the Jeans mass in order to resolve fragmentation physics. One reason is that the relevant quantity would be the *turbulent* Jeans mass and not the *thermal* Jeans mass because the cold and warm interstellar medium is supersonically turbulent. The former is often of order 10^7 $M_\odot$ and is thus well resolved. Plus the Jeans mass is the smallest scale at which fragmentation happens, all larger scales are also unstable. The relevant scale to resolve in order to capture fragmentation is the Toomre scale [Toomre, 1964].

2 The CHIMES programme

The GIZMO code included in the FIRE set-up uses a lot of pre-tabulated cooling rates when it is dealing with gas particles. Those values assume chemical equilibrium within the gas cell and have a sufficient precision if one does not look at the exact chemical properties of the gas. The FIRE code only knows the mass fraction corresponding to each element (Hydrogen, Helium, Nitrogen, Oxygen, Neon, Magnesium, Silicon, Sulphur, Calcium, Iron, electrons. Mass fractions of other elements can also be tracked, but not by default and this has to be specified when running GIZMO.). It also tracks how much hydrogen is ionised. However in order to make line-intensity predictions, one has to know precisely the abundance of a given type of molecules. I thus also used the CHIMES chemistry abundance solver [Richings et al., 2014a,Richings et al., 2014b]. It can use the data from the FIRE simulation in terms of metallicity of the interstellar medium gas and compute the quantity of a lot of different chemical compounds that can be formed with basic elements of the interstellar medium gas.

The main difference between the chemistry done by CHIMES and the quick computation that FIRE does on-the-fly is that FIRE only solves for the mass fraction of each elements. The CHIMES code assumes chemical equilibrium and solves the problem in a finer way: using chemical species rather than just atoms. The script runs in each cell until the equilibrium is reached. However CHIMES is run after FIRE as a post-processing step. There might be some slight differences between running CHIMES afterwards and the real chemical out-of-equilibrium state. However running it at each step of the FIRE run would be very resource and time demanding.

[1]Those very high resolution runs are available only for dwarf galaxies of mass $\lesssim 10^{10}$ $M_\odot$.
[2]When the halo mass is indicated, it is the halo mass at redshift 0. The halos at redshift 6 will have a lower mass as they had less time to grow.

2.1 Chimes parameters

When one wishes to compute the abundances of a lot of chemical species, one has to take at lot of external parameters into account. The two most important of them are the UV field and the gas shielding length.

Ionising UV field Ultra-Violet radiation plays an important role in determining the abundances of chemical species. UV photons can ionise atoms and molecules and depending on their energy they sometimes can break molecules apart. For example, the two following reactions can happen in the interstellar medium and require high-energy UV photons.

$$\mathrm{H} + \gamma \rightarrow \mathrm{H}^+ + e \tag{1.1}$$
$$\mathrm{H}_2 + \gamma \rightarrow 2\mathrm{H} \tag{1.2}$$

Where γ is a photon with a big enough energy, and e is an electron. Chimes has two default UV field modes. Both of those are homogeneous background fields that does not depend on the stars or other radiations sources in the galaxy, they are completely independent of the simulation. The first one is the extra-galactic field which takes into account only the UV radiation coming from outside the halo disk, for example from other galaxies. The second one is a background field corresponding to a usual galactic background due to the stars inside it. This field does not depend on where the stars actually are in the galaxy nor does it depend on their density, and other properties. This field was calculated independently of the simulation run and data.

It is also possible to use a modulated field that is computed by gizmo taking into account the positions of the star cells in the simulated box. However this field is not printed by default by gizmo and one has to rerun gizmo for a few steps in order to get it, which is time consuming. I examine the influence of the change of the uniform UV field to the modulated UV field in chapter 3.

Shielding length One has to keep in mind that even though the fire simulation is a *high resolution* simulation, a lot of small scale physics is not resolved. For example, the typical interstellar medium gas cell within a galactic disk has a size of the order of a few parsecs at bests. Local gas clumping due to different phenomena is not being taken into account and all we have is the average density of the gas cell. Turbulence is also far from being resolved in this simulation and both of these phenomena can dramatically change the shielding length of gas.
The shielding length is an important parameter as it will strongly influence the received emission and depends on the local density. It corresponds to the typical attenuation length of the light intensity going through a medium due to absorption. The different mechanisms giving rise to different lengths are detailed below. Gas shielding has two main effects. The first one is that the gas will absorb photons and this will obscure the images. The second, and most important effect, is that the gas will be protected from radiation. There will be less ionisation and radiation-due dissociation.

When looking at inhomogeneous media from a given perspective (for example the crab nebula gas seen from earth), the relevant quantity is often the column density rather than the density. It is defined

$$\Sigma = \int_{\mathrm{LoS}} \rho ds \tag{1.3}$$

where Σ is the column density and ρ is the density which is integrated along the line of sight. This definition of the column density can be used to define the shielding length L, such that

$$\Sigma = \overline{\rho} L \tag{1.4}$$

where $\overline{\rho}$ is the mean density along the line of sight or, for example, in a gas cell. Let us go through some physical phenomena that can have an impact on the shielding length [Richings et al., 2014b].

Jeans' instability One of the simplest thing that can happen to an homogeneous self-gravitating gas cloud is that it collapses. One can compute the maximum radius of a homogeneous gas sphere undergoing its own gravity before it collapses.

$$L_J = \sqrt{\frac{15kT}{4\pi G\rho\mu}} \tag{1.5}$$

where k is Boltzmann's constant, G is Newton's constant, T is the gas temperature, ρ its density and μ the mass of the particles of the gas (for example hydrogen atoms). Such a collapse could change the shielding length because, for instance the gas in the cell could not actually be homogeneous but rather be in small dense balls of gas that collapsed and the rest of the cell would be almost empty. In this case the shielding length would be very different inside the dense gas or between the clumps.

Density variation Like in the previous scenario, the density could be very inhomogeneous. This could be because of turbulence in the gas cloud for example. A way to obtain the typical length scale on which the density varies in that case is simply

$$L_\rho = \frac{\rho}{|\nabla \rho|} \tag{1.6}$$

where ρ is the local density of the gas (we no longer assume the gas to be homogeneous).

Thermal line broadening One can define a similar length scale for velocities variation within the gas.

$$L_{\text{Sobolev}} = \frac{v_{\text{th}}}{|\nabla v|} \tag{1.7}$$

This for length scale corresponds to the distance at which the absorption profiles will be shifted by one local linewidth. This length scale was first defined by Sobolev in [Sobolev, 1957].

All of the previous length scales can be used as the shielding length for the Chimes programme in order to try to do better than the actual resolution of the fire simulation when looking at the interstellar medium chemistry.

3 Computing luminosity with RADMC-3D

Most astrophysical objects, like galaxies, stars, are surrounded by dust and gas. If sometimes this dust and gas can completely obscure the light coming from those object for earth observations, the light emitted by the gas and dust are often not negligible sources, even when some direct light can be observed. The gas and dust is heated by the high-energy photon-light from the local stars and then reemits the energy at longer wavelengths. In order to reproduce images comparable to observations, one shall model all the absorption and reemission phenomena. This problem is known as the radiative transfer problem.
To solve this problem, *i.e.* find at each point of space, for each direction and wavelength of interest the value of the specific intensity I_ν (in the CGS-system, its unit is erg/s/cm^2/Hz/sr), I used the radmc-3d programme. The radiative transfer equation is the following.

$$\frac{dI_\nu}{ds} = -\alpha_\nu I_\nu + j_\nu \tag{1.8}$$

where s is the coordinate along the ray (or line of sight), I_ν is the specific intensity, *i.e.* the emitted light flux at frequency ν per unit solid angle (it is thus constant along a ray if there is no source nor dissipation), α_ν is the dissipation coefficient at frequency ν (it is often due to absorption and it is the inverse of the mean free path of photons due to dissipation), and j_ν is the source term, called emissivity.
The above equation is the simplest form of the radiative transfer equation. It often is more complicated, as the specific intensity may influence the gas or dust temperature which then modifies the way the gas or dust absorbs or emits light. For instance, atomic line or black-body emission depend on the temperature of the emitting body. We can also decompose the source and dissipative terms.

$$\alpha_\nu = \alpha_\nu^{\text{abs}} + \alpha_\nu^{\text{scat}} \tag{1.9}$$
$$j_\nu = j_\nu^{\text{abs}} + j_\nu^{\text{ther}} \tag{1.10}$$

where we decomposed the dissipative term in an absorption part as well as a scattering part. The source term is also decomposed in a scattering term and a thermal emission term.

As the name would suggest, the way in which radmc-3d solves this equation is by using a Monte-Carlo scheme, more precisely an immediate reemission Monte-Carlo scheme described in [Bjorkman and Wood, 2001]. Photons are emitted and followed in their interactions. When a photon packet is absorbed its energy is added to the envelope and an new photon is immediately emitted taking into account the temperature modification due to the absorption of the first photon [Pascucci et al., 2004]. This methods implicitly conserves the total energy. As the photons are emitted stochastically, one has to take a sufficiently big number of emitted photons for them to cover all the volume of interest. However the method proposed by Bjorkman and Wood [Bjorkman and Wood, 2001] has some problems. It creates noisy temperature profiles in optically thin media [Pascucci et al., 2004], this is a real problem if one wishes to look at galacatic interstellar medium gas. To solve this problem, C. P. Dullemond[3] *et al.* chose to treat absorption partly as a continuous process, as proposed in [Lucy, 1999].

4 Image stacking – Observational mocks

4.1 Noise

In order to produce data that can be compared to observations, one need to add noise. Here I added random gaussian noise on each pixel of the image rendered by RADMC-3D. The probability distribution of such a noise is a gaussian function for each pixel.

$$\forall x \in \mathbb{R}, P(X = x) = \frac{1}{\sqrt{2\pi\sigma^2}} e^{-\dfrac{x^2}{2\sigma^2}}, \tag{1.11}$$

where X is the random variable and σ is the standard deviation of the distribution. I assume every random variables, the X's, for each pixel, to be independent. One can notice that this gaussian distribution is centered around zero. This means that the noise is as likely going to reduce the intensity in one pixel as it is going to increase it. This kind of noise is the one reported in [Fujimoto et al., 2019] and is the simplest one when one has no prior information on the physical noise source. I tune the standard deviation of the probability distribution to match the standard deviation of observations reported in [Fujimoto et al., 2019].

The noise levels reported there are around $\sigma = 25 \quad \mu\mathrm{Jy}$.

4.2 Beam

The second step to produce observation-like data is to take into account the influence of the telescope beam. Here I chose the simplest beam: a gaussian beam. The expression of such a beam is simply a two-dimension gaussian function $W(x, y) = \frac{1}{\sqrt{2\pi\sigma^2}} e^{-\frac{x^2+y^2}{2\sigma^2}}$. It is important to normalise the function, because otherwise the total intensity would not be conserved.
The way to model the influence of the beam on the signal is to convolve the signal and the beam window function.

$$S_B(x, y) = (S * W)(x, y) = \iint S(u, v) W(x - u, y - v) du dv, \tag{1.12}$$

where W is the window function, S is the signal function and S_B is the *beamed* signal function. For a gaussian beam, I use the definition of the beam size in agreement with [Fujimoto et al., 2019]. I define the size of the beam to be the full width at half maximum of the gaussian function.

4.3 Stacking

In [Fujimoto et al., 2019], Fujimoto *et al.* use a stacking method in order to reduce the noise level of their observation sample. Here I use a similar technique. As they have observational data, the noise level of each galaxy observation is different and they choose to make a noise-weighted average for their stack. Here the noise levels are the same, so I take the median value for each pixel. The median is more "scale independant" than the average, *i.e.* the highest values will not suppress the influence of lower values.

One also has to choose the stack position, *i.e.* how should the common centre be chosen. Fujimoto *et al.* used the maximum of rest-frame UV intensity. To be consistent with that choice, I chose the maximum of projected and beamed star mass for each orientation. The UV observation reported in that paper also comes from ALMA observations. I use a gaussian beam similar to the one of ALMA to beam the projected star mass map, in order to reproduce what they would have seen had they been looking at those galaxies with ALMA. The reason to do so is that UV are mostly emitted by young stars and if we assume that most of the stars formed around $z = 20$, they would only be 700 million years old by $z = 6$. One could have also chosen where the star formation rate is the highest in the galaxy, because that is where most young stars would be. The problem in doing so is that if there is a violent event in the halo, for example a supernova, a lot of gas would be expelled. The local star formation rate would then dramatically drop, because the gas density would be very low. However, the stars would not have been expelled by the supernova explosion, and the UV emission would be in a low star formation rate area.

[3] The main contributor to RADMC-3D. The reference paper is still in preparation for the 3D version. See http://www.ita.uni-heidelberg.de/~dullemond/software/radmc-3d/.

Chapter 2

Results – General : The general properties of redshift 5 – 7 galaxies

Galaxies at redshift 5–7 (*i.e.* between 0.7 and 1.2 billion years after the big bang) are hard to study. The first reason is that those galaxies are often too dim to be observed and resolved to a satisfying quality. The first observation of such galaxies with the [C_{II}] line were obtained by looking at lensed galaxies, for example [Bradač et al., 2017]. Now that the ALMA telescope is online, it is possible to have a good enough resolution for [C_{II}] individual galaxies observations at redshift 5 to 7 [Aravena et al., 2016, Smit et al., 2018, Fujimoto et al., 2019]. Stimulation can also be a useful tool to match the observed properties of those galaxies with more difficult ones to obtain from observation that one could obtain with simulations.

1 Relevant quantities

There are several properties of galaxies and halos that are worth looking at. I first studied properties of high redshift galaxies to find a consistent way of studying those properties. The code I wrote can then be used on any galaxy that I will later study. I compared the data I got from the simulations to data from reference articles and to observational data.

1.1 Star formation rate

This quantity is the mass of star that is created by unit of time. The usual unit is $M_\odot$/yr. It is computed by the GIZMO code for each gas cell. The star formation process requires a high gas density and thus all gas cells do not create stars at each time step. As the star formation rate highly depends on the gas density, there is often only a few gas cells that are effectively forming star at each time step. It is thus not really relevant to look at the quantity for each and every cell. The relevant way to examine the star formation rate is to sum it over a halo region. The total star formation rate can be linked to the [C_{II}] emission in a simple way [De Looze et al., 2011, Lupi and Bovino, 2019, Boselli et al., 2002, Lagache et al., 2018, Carniani et al., 2018], but this requires to know the [C_{II}] emission and not only the C_{II} mass.

1.2 Stellar mass and halo mass

Another quantity that is of interest is the relationship between the stellar mass of halo and its total mass *i.e.* with the dark matter and the gas as well as the stars of the halo. This has been the subject of many papers in the last years as simulations tend to show that there is a simple double power law relationship between them [Bjorkman and Wood, 2001, Moster et al., 2012]. Knowing how those two quantities are related would be very useful for observations as we are usually only able to look at the stars. The gas of the halo being too dim and the dark matter not being visible, this would enable us to have an estimate for their mass. Figure 2.3 is one of those plots, it include literature values fits as well as points corresponding to the halos I have been studying at redshift 6.

1.3 Surface density

The surface density of a halo is the quantity that is the simplest to picture. It is the density per surface area (annulus-shaped slice of the halo) as a function of the radial position with respect to the centre of the halo. This quantity can inform us on the messiness of the halo and the position correlation of star and gas.

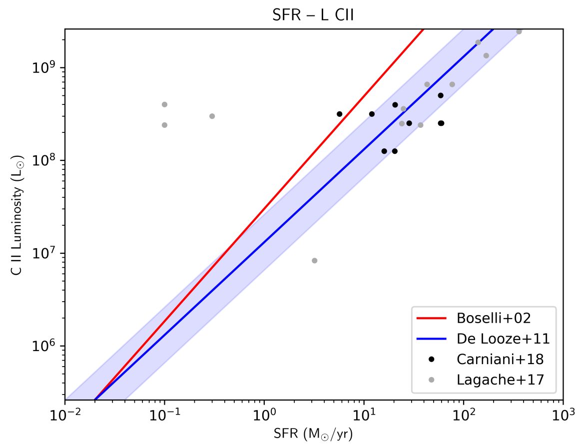

Figure 2.1: Here is a plot of some of the observed data presented by De Looze [De Looze et al., 2011], Lagache [Lagache et al., 2018], Carniani [Carniani et al., 2018] and Boselli [Boselli et al., 2002]. The red and blue lines are the fit proposed in the papers. The light blue area corresponds to the error on the fit by De Looze *et al.* The observational data tends to show that there is a relationship between the star formation rate of a galaxy and its [C_{II}]-line luminosity. The data from [De Looze et al., 2011,Boselli et al., 2002] are for local dwarf galaxies whereas the data from [Lagache et al., 2018,Carniani et al., 2018] are from high-redshift galaxies.

1.4 Metallicity

The metallicity is maybe the most important quantity to look at when one wishes to look at line emission of a specific molecule or ion. It is the mass fraction of the gas or star of a given element. Here and as is it often the case in astrophysics, we call metal all element heavier than Helium. This will enable us to know the quantity of each element in each gas cell which can then be used to compute the quantity of a given molecule. For example the quantity of oxygen and carbon atoms will be related to the quantity of carbon monoxide (CO) in a given gas cell. This can then be used to predict the intensity of the emission line of a chosen molecule or chemical species. As can be seen on figure 2.2 there is a relationship between this quantity and the stellar mass in halos.

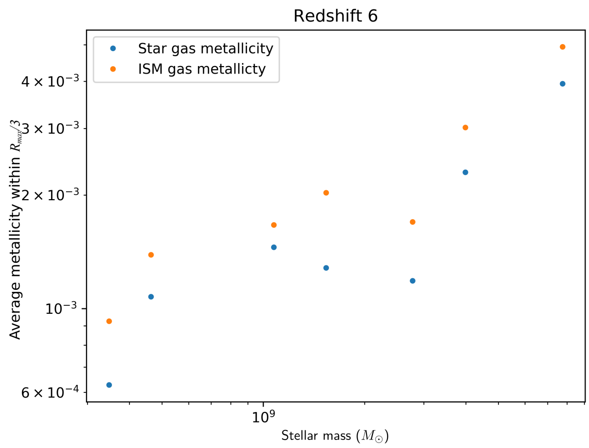

Figure 2.2: Here is a plot of the average metallicity of the gas around the halos versus the stellar mass of the halos. The orange circle are for interstellar medium cold gas ($T \leq 300$K) and the blue circle are for star heated gas ($T > 300$K). $R_{\max}$ is the radius at which maximal circular is reached in the halo.

1.5 Centre of mass

Looking at the position of the centre of mass of a halo can also be interesting. It is also interesting to look at the centre of mass of a given type of particle and then compare the different centre of mass.

2 Summary of the properties of $z = 5$–7 galaxies

In the simulations the halos at redshift 5 to 7 are often quite messy. The gas is often not spatially organised whereas the stars tend to be part of 1 kpc structures. The spatial distribution of gas and star depends only little on the redshift. At those redshifts, the gas tends to be where the stars are not *i.e.* further away from the halo centre, making a hole of about 10 kpc for the stars. Although as times goes by the halos tend to be more organised, in particular the stars. The star centre of mass and the gas centre of mass tend to be different by a distance of the order of 1 kpc. I also noticed that the gas centre of mass and the dark matter centre of mass are almost always the same.
The star formation rate increases with time as does the metallicity of star-heated gas (T $>$ 300 K) and cooler interstellar medium gas. Yet the interstellar medium gas tends to have a slightly higher metallicity.
The stellar mass to halo mass relationship seems to be behaving as models from literature predict as can be seen on figure 2.3. It fits very well the fit provided by Ma *et al.*, this was to be expected as this fit was made from FIRE simulation points. Yet it also behave like models independent of the FIRE simulations at redshift 6.

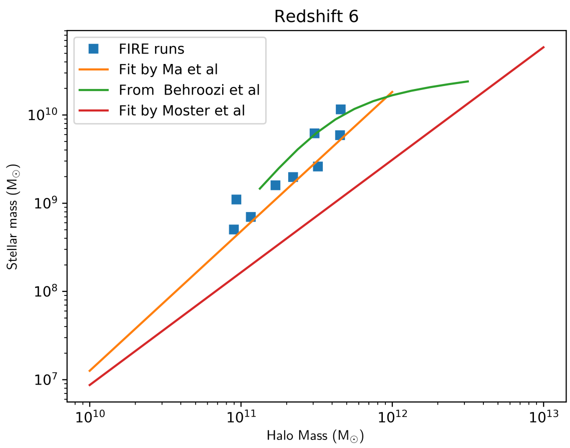

Figure 2.3: This is the stellar mass to halo mass relationship for galaxies at redshift 6. The solid lines correspond to fit to observations from Behroozi *et al.* [Behroozi et al., 2013] and Moster *et al.* [Moster et al., 2012]. I also plot a fit proposed by Ma *et al.* [Ma et al., 2018b] for the FIRE simulation at redshift 6.

It is also very helpful to look at projection plots of the gas and star particles to see the actual shape and structure of the halos. See figure 2.4).

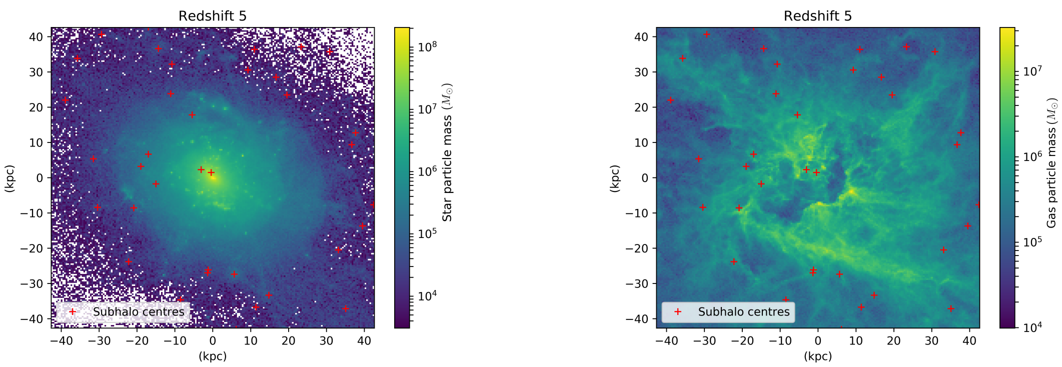

(a) Star distribution. **(b)** Gas distribution.

Figure 2.4: Here we can see the spatial projection of the gas and star particles and their mass. The red crosses indicate the centre of subhalos which were found using the Amiga Halo Finder (AHF) programme [Gill et al., 2004, Knollmann and Knebe, 2009]. On both plot the size is in comoving kiloparsecs. **Left:** The star scatter of the halo. The colourbar shows the mass of star particles in each bin (a bin is approximately 0.43×0.43 comoving kpc). **Right:** The plot is very similar to the previous one, here it is the gas mass.

3 Galactic interstellar medium properties

One can use the abundances provided by the Chimes code to look at the global properties of the halos. Similarly to the gas density maps that can be done using the FIRE raw output, here it is for example possible to plot the molecular density of CO, C_{II} H_2, and all the other chemical species that Chimes uses.
It is interesting to plot the phase diagram of different Carbon species. We can see that each of the species lies in a different place of the temperature-density space (figure 2.5). One can also look at the maps and surface density radial profiles of the molecules at hand. Those plots give redundant information but only some of them can be observed from earth or with space telescopes. It is then possible to use the data from simulation to guess some non-observable quantities of observed halo, assuming that they behave like the one of the simulations.
As I will be looking at the $[C_{II}]$ line emission, it is interesting to see what are the conditions for C_{II} to be present in the interstellar medium, for example at which temperature ranges and which density it is stable.

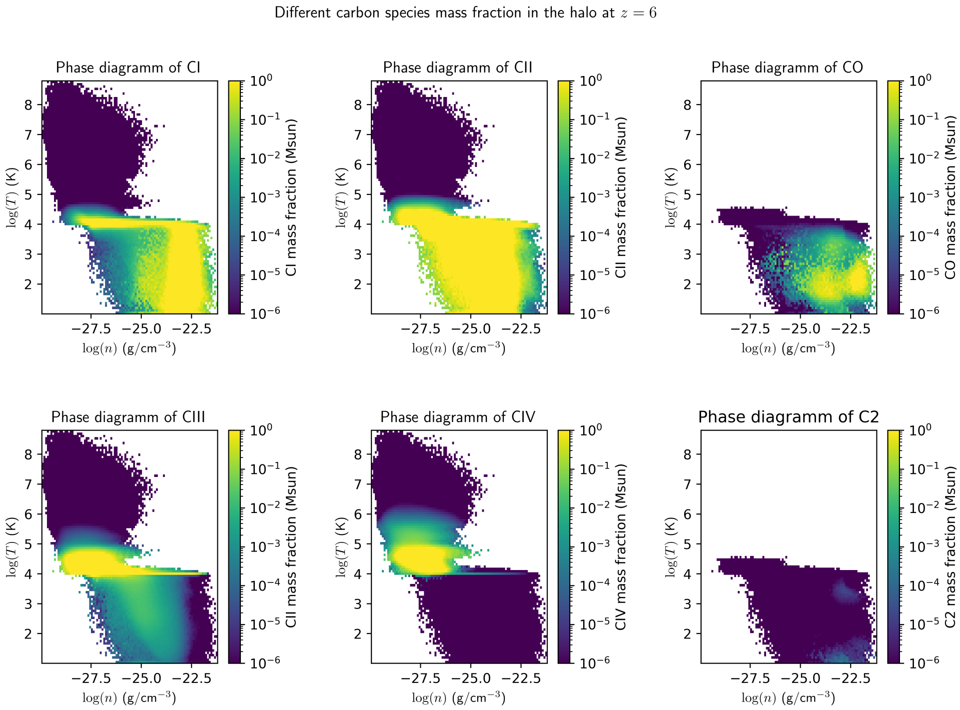

Figure 2.5: The phase diagram of the most abundant carbon molecules. The colour shows the fraction of the total carbon mass in each FIRE cell. If we sum all the fractions of all the species, it adds up to 1 for each bin of the histogram. For example one can see that the more ionised the carbon atom is, the higher the temperature at which it lies has to be.

However, most of the observed quantities are directly linked to the luminosity rather than to simply the density and temperature. It is then necessary to compute the luminosity of the halos we wish to study. We will examine such relationships in the next chapter. Nevertheless the gas distribution and properties will have an effect on the $[C_{II}]$-line luminosity. Indeed, most of the $[C_{II}]$-line emission comes from the densest regions. The regions with low density even if they might be responsible for a bigger part of the total C_{II} mass of the halo, will have a lower luminosity.

Chapter 3

Results – [C_{II}] halos at redshift 6

The 158μm-[C_{II}] emission line corresponds to the deexcitation of ionised carbon from its only excited state to its fundamental state. However carbon is not natural in its C_{II} form and has to be ionised from atomic neutral carbon. The two main ionisation mechanisms are collisions and ionising radiations, for instance UV photons.

1 The influence of the local ionising UV field

There are several ways to model the UV field in the interstellar medium. One can assume that the UV field is uniform, by taking an average value for the field. This field value can be the one created by the stars of the halo, but in some cases, one wishes to look at the influence of the extra-galactic UV background.

Here I compare the radial surface density of different carbon and hydrogen species. In the first case I use a uniform UV field corresponding to the homogeneous UV field inside a galaxy (dashed line on figure 3.1). In the second case I use a modulated UV field (solid line). The modulations of its value is given by GIZMO if requested in the computation, this field's value depends on the star positions. In the second case I also add the extra-galactic average field to the modulated one. On figure 3.1 one can see the influence of the change in UV field. The consequence of having a modulated field compared to a uniform intra-galactic background is that the ionising field is weaker in the outskirts of the halo in the former case as there only are a few stars there.

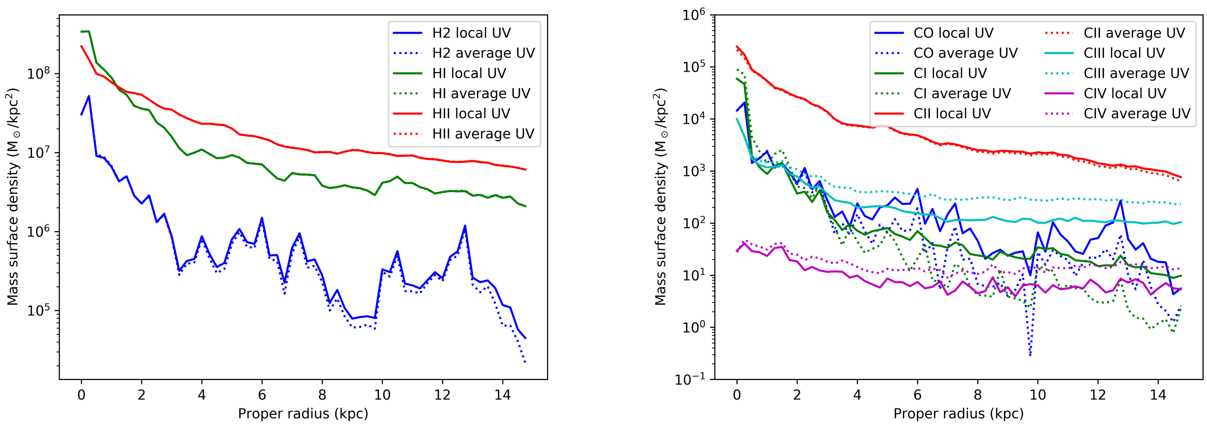

(a) Hydrogen species. **(b)** Carbon species.

Figure 3.1: Here are plotted the radial surface density of several hydrogen and carbon species that I obtained. **Left:** The most present hydrogen species are H_2, H_I and H_{II}. We see that the radial distribution of H_I and H_{II} does not change with the modulated field. However the H_2 molecules are less likely to get dissociated by UV photons in the outskirts of the halos with this field. **Right:** Here are plotted the radial distribution of the most important carbon species. We see that the highly-ionised species require a high UV field to be ionised, whereas C_I, C_{II} and CO seem to be more stable with a weaker field in the outskirts of the halo.

We notice that in the centre of the galactic halo (in the innermost 2 to 4 kiloparsecs) there is not much change. This was to be expected as the value of the UV field did not change by a lot there. However in the outskirts of the halo (from 4 to 15 kiloparsecs away from the centre), there is less ionised species and more neutral carbon and hydrogen. This trend is however not exact as there is more C_{II} in the outskirts of the galaxy when the UV field is weaker there. The explanation could be that with a weaker ionising field carbon stays singly ionised and the higher ionised stated are more difficult to reach.

2 [C_{II}] emission

As explained in the previous chapter, there is a way to easily compare the [C_{II}] emission to observations. One can make use of the $L_{[C_{II}]}$–SFR relationship reported from observations [De Looze et al., 2011].

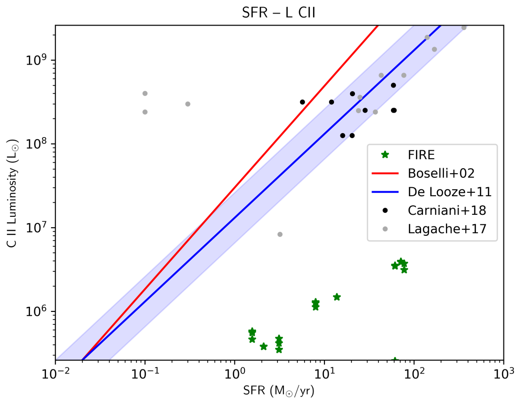

Figure 3.2: Here is the $L_{[C_{II}]}$–SFR relationship with the points corresponding to the halos I am studying at redshift 6. As we can see the points are somewhat off the fit proposed in the literature.

As can be seen on figure 3.2 the points corresponding to the FIRE halos seem to be off the usual fit provided by the literature. At this point I still am trying to investigate this. The luminosity seems to be too weak for SFR that are comparable to observed for galaxies of this size.

3 [C_{II}] emission 10-kpc radial extension

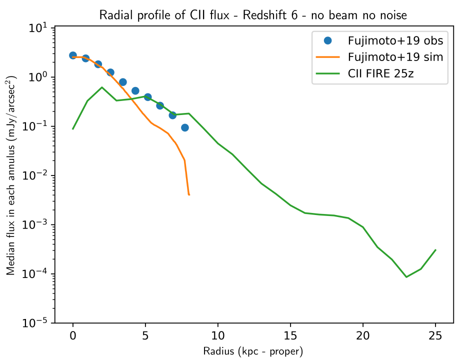

Figure 3.3: Here is a radial profile for *only one* halo, that happens to approximately fit the observed data. No stack has been done at this point. In green this is the radial surface flux of [C_{II}] light, In blue is plotted the observation reported in [Fujimoto et al., 2019]. In orange is plotted the simulated result of the same reference.

Figure 3.3 represents a radial profile for only one halo. Neither noise nor beam effect has been applied to the flux map used for the radial profile. This preliminary result has to be taken with some care as it probably is not representative. Yet it shows a feature present on all halos I am studying which is the large spatial extension (*i.e.* the flat slope on the outskirts of the halo). Consistently with figure 3.2, we see that the [C_{II}] luminosity is not as high as the halos reported in [Fujimoto et al., 2019].

4 Possible scenarios

The work is aiming to investigate whether the scenarios proposed by Fujimoto *et al.* in [Fujimoto et al., 2019] are plausible and reproduced in the FIRE simulations set at the same redshift.

4.1 Satellite galaxies

Let us first examine the satellite-galaxy scenario (scenario a) in the list in the introduction. As we saw previously with figure 2.4, AHF enables us to easily find the halos and subhalos in one FIRE run. I look whether there is a correlation between the subhalos positions and where there is a lot of C_{II}, using both AHF[1] results and CHIMES outputs.

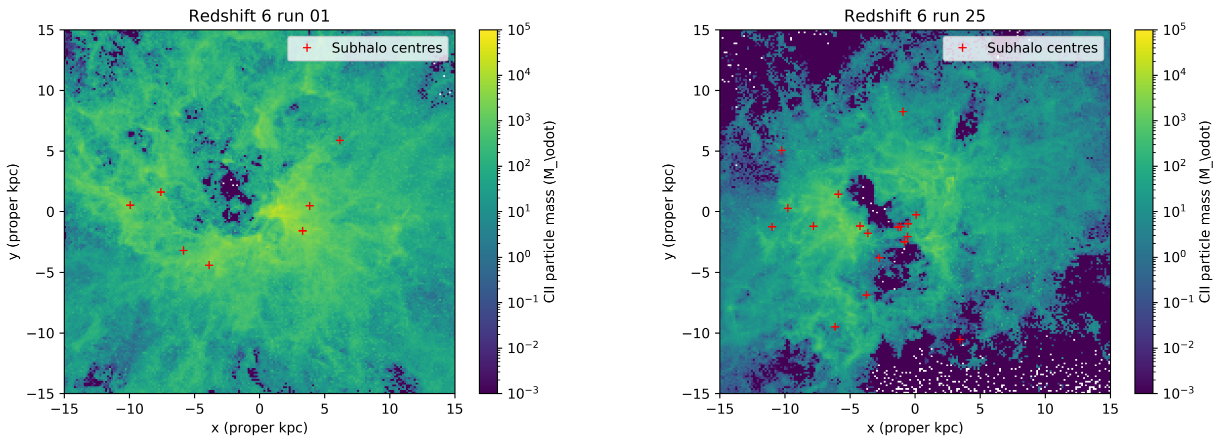

Figure 3.4: Here are two plot of the projected C_{II} mass (colourbar) and the subhalo positions (red crosses). We can see that there is no obvious correlation between the two quantities. Those two plots are taken from a bigger set of 27 (9 halos × 3 axes). There was no correlation on the whole set.

On figure 3.4 we can see no obvious correlation between subhalos positions and C_{II} distribution. This indicates that the satellite galaxies scenarios is not likely explaining the presence of [C_{II}] emission on a large scale.

4.2 Outflows

A scenario that seems more plausible for the FIRE simulations set with which I am working is outflows (scenario e). Figure 3.5 tends to show that the gas has be expulsed from the central star halo. This could be due to feedback effect such as violent supernovæ .
In every halo the stars are packed at the centre of the halo within a few kiloparsecs. The gas is often distributed in a messier way, and very often there is less of it in the centre of the halo *i.e.* where the stars are. Different shapes of the gas distribution can be caused by different feedback effects. It is also possible that for some halos, there was no supernova for a long time and the gas had some time to fall back towards the stars. The place where the alleged supernovæ happens can also have an important impact on the shape of the gas distribution. It is very possible that a supernova happens on the edge of the star halo, thus blowing all the gas in mostly one direction. In [Fujimoto et al., 2019] they also present an attempt to reproduce the spatial extension of [C_{II}] halo with simulation. They report to be unable to do so. This could be because the feedback implemented in their simulation is not able to produce violent enough feedback phenomena.

4.3 Cold streams

With FIRE simulations it is also possible to examine whether there are cold streams (scenario d). Here I look for coherent gas flows with an inwards radial velocity. If the radial velocity map of the halos consistently shows concentrated spots with high rate of incoming gas this will be a sign that this scenario is plausible. A radial velocity map is plotted on figure 3.6.
As is shown on figure 3.6 there is no obvious sign of coherent streams of gas inflowing in the halo. We can not totally rule out this scenario but it is unlikely for it to be the main mechanism bringing C_{II} on a much larger scale than the star halo.

[1] AmigaHalo Finder – Adaptive Mesh Investigations of Galaxy Assembly.

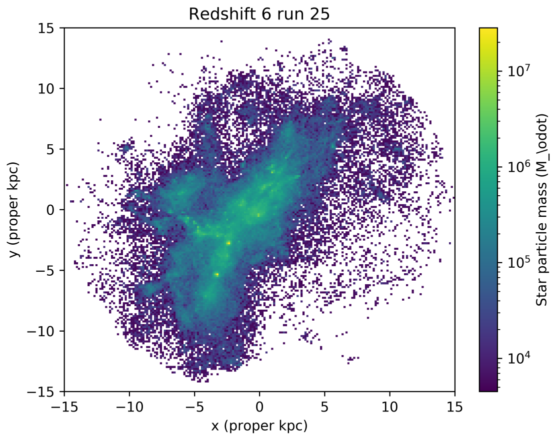

(a) Star distribution.

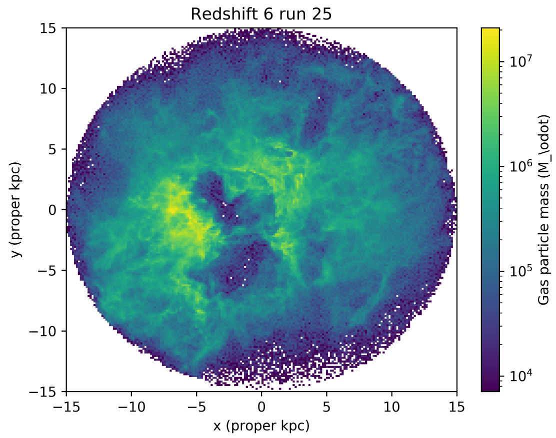

(b) Gas distribution.

Figure 3.5: Here are a plot of the star mass projection and a plot of the gas mass projection. I chose this halo as it is very clear that most of the gas is outside the star halo, meaning that it could have been expelled. A similar behaviour can be observed throughout the whole halo set. Both plots are projection plots of the mass of star or gas within a 15 (proper) kpc sphere.

The two other scenarios are harder to investigate with the FIRE simulations as Fujimoto *et al.* do not provide a physical origin for the large photo-dissociation region or the presence of ionising photons on a larger scale than the star halo. A way to do so could be looking at the Lyman-α emission of the halo to try distinguish either of those scenarios. I leave this open for future works. From what I observed, the most likely scenario is outflows. Supernovæ explosion are known to have influence across the whole halo they are in. One of them could expel a lot of C_{II} containing gas on a much larger scale than the central star halo.

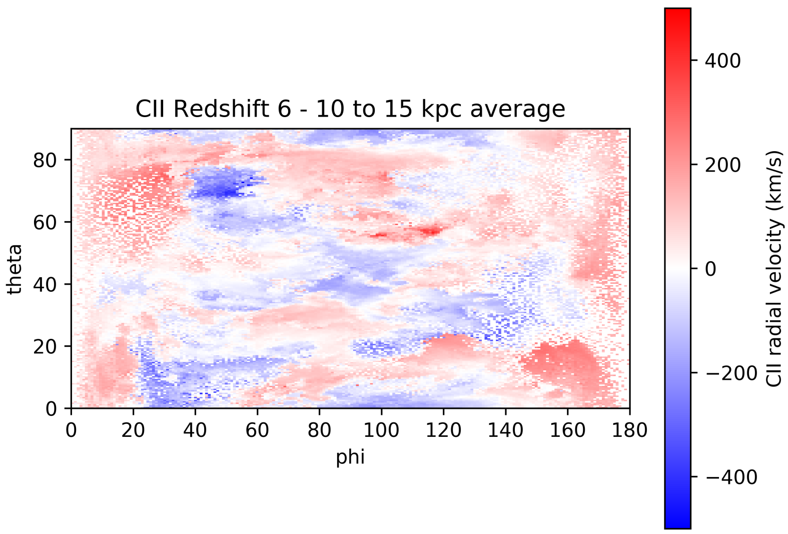

Figure 3.6: Here is a radial-velocity map for one halo. The velocity in each angular bin has been averaged on the 10^{th} to 15^{th} radial kiloparsecs and weighted by the C_{II} mass of the gas particles (as this is what is observed). This is where the cold stream should be seen, lowering the influence of the inner galaxy dynamics. Negative radial velocity indicates inflow and positive radial velocity stands for outflows. What can be seen here is turbulent gas motion. There is no sign of coherent stream feeding the gas halo.

Chapter 4

Conclusion

In this report I present how it is possible to study the formation of galaxies with numerical simulations from early universe conditions. I focused on ways to reproduce [C_{II}] observations of high redshift galaxies as simulations of [C_{II}] emission can help understand those observations. In order to have a sensible reproduction of the physics of the interstellar medium one needs to use galaxies simulated in a realistic environment thanks to the FIRE simulations. Then one also has to include the interstellar medium chemistry as the lines that we can most easily detect do not come from atomic elements. Plus taking chemistry into account gives more precise results on the abundances of the species of interest. Then to model the actual line emission of the interstellar medium one needs to solve the radiative transfer problem in the whole halo we wish to study.
Those techniques enable us to first examine the most general properties of the high-redshift galaxies, and by so doing checking that the simulated FIRE halos are comparable to the ones that we observe at redshift 5 to 7.
Finally, we look at more precise properties of the halos aiming to reproduce observations reported by Fujimoto *et al.*. The preliminary results seem to show that the reported spatial extension of the [C_{II}] emission halo is also present in the FIRE simulation. However the luminosity of those halos do not match the observations. I then examine the plausibility of the scenarios proposed by Fujimoto *et al.*

Fujimoto *et al.* proposed five scenarios that could explain why there is [C_{II}] emission in a much larger scale than the central star halo. The stars are expected to be the sole source of high enough energy photons to sustain a high mass fraction of ionised carbon in its C_{II} form. I investigate three of those scenarios thanks to the techniques presented in this report.
The first one to be at least partially ruled out in the FIRE simulations is the satellite galaxies scenario. The existence of subhalos around one main halo allegedly explains the existence of C_{II} on a large scale. Although subhalos were present in the FIRE simulation, their position do not correlate in any way to the C_{II} distribution. This scenario can not be definitively ruled out at this point, but should not play a major role in the size of large [C_{II}] halos.
Then I also set aside the possibility that cold streams, that are known to feed high star formation rate in early galaxies, explain large scale [C_{II}] emission. There is no proof of such stream for the halos I have been studying. Here too, this scenario can not be completely be ruled out because of the small sample of halo I am working with, but it should not be the leading process.
The most likely scenario is outflows. A lot of feedback effects have been implemented in the FIRE set-up and violent ones like supernovæ could explain large [C_{II}] emission scales. A supernova in the central star halo can blow gas kiloparsecs away. I present some plots showing evidence that the gas of the halos has been expelled from the centre of the halo.

The FIRE simulation are able to reproduce the spatial extension of reported [C_{II}] emission. while the Althæa simulation does not [Fujimoto et al., 2019]. This could also be a way to test feedback model for galaxy formation and evolution.

Although the result I present here are promising, there still is work to be done. First the low [C_{II}] luminosity has to be explained for this simulation set. Then a way to confirm that violent feedback effects as supernovæ are causing is to rerun the same simulations but with the supernova rate lowered of set to zero. This is left for future work.

Bibliography

[Aravena et al., 2016] Aravena, M., Decarli, R., Walter, F., Bouwens, R., Oesch, P. A., Carilli, C. L., Bauer, F. E., Cunha, E. D., Daddi, E., Gónzalez-López, J., Ivison, R. J., Riechers, D. A., Smail, I., Swinbank, A. M., Weiss, A., Anguita, T., Bacon, R., Bell, E., Bertoldi, F., Cortes, P., Cox, P., Hodge, J., Ibar, E., Inami, H., Infante, L., Karim, A., Magnelli, B., Ota, K., Popping, G., van der Werf, P., Wagg, J., and Fudamoto, Y. (2016). The ALMA spectroscopic survey in the hubble ultra deep field: Search for [c ii] line and dust emission in $6 < z < 8$ galaxies. *The Astrophysical Journal*, 833(1):71.

[Behrens et al., 2018] Behrens, C., Pallottini, A., Ferrara, A., Gallerani, S., and Vallini, L. (2018). Dusty galaxies in the Epoch of Reionization: simulations. *Monthly Notices of the Royal Astronomical Society*, 477(1):552–565.

[Behroozi et al., 2013] Behroozi, P. S., Wechsler, R. H., and Conroy, C. (2013). The average star formation history of galaxies in dark matter halos from $z = 0$-8. *The Astrophysical Journal*, 770(1):57.

[Bjorkman and Wood, 2001] Bjorkman, J. E. and Wood, K. (2001). Radiative equilibrium and temperature correction in monte carlo radiation transfer. *The Astrophysical Journal*, 554(1):615–623.

[Boselli et al., 2002] Boselli, A., Gavazzi, J., and Pierini, D. (2002). [cii] at 158 μm as a star formation tracer in late-type galaxies. *A&A*, 385:454–463.

[Bradač et al., 2017] Bradač, M., Garcia-Appadoo, D., Huang, K.-H., Vallini, L., Finney, E. Q., Hoag, A., Lemaux, B. C., Schmidt, K. B., Treu, T., Carilli, C., Dijkstra, M., Ferrara, A., Fontana, A., Jones, T., Ryan, R., Wagg, J., and Gonzalez, A. H. (2017). ALMA [c ii] 158μm detection of a redshift 7 lensed galaxy behind RX j1347.1-1145. *The Astrophysical Journal*, 836(1):L2.

[Carniani et al., 2018] Carniani, S., Maiolino, R., Amorin, R., Pentericci, L., Pallottini, A., Ferrara, A., Willott, C. J., Smit, R., Matthee, J., Sobral, D., Santini, P., Castellano, M., De Barros, S., Fontana, A., Grazian, A., and Guaita, L. (2018). Kiloparsec-scale gaseous clumps and star formation at z = 5–7. *Monthly Notices of the Royal Astronomical Society*, 478(1):1170–1184.

[Croton, 2013] Croton, D. J. (2013). Damn you, little h! (or, real-world applications of the hubble constant using observed and simulated data). *Publications of the Astronomical Society of Australia*, 30:e052.

[Dayal and Ferrara, 2018] Dayal, P. and Ferrara, A. (2018). Early galaxy formation and its large-scale effects. Physics Reports, Volumes 780 to 782, 5 December 2018, Pages 1 to 64.

[De Looze et al., 2011] De Looze, I., Baes, M., Bendo, G. J., Cortese, L., and Fritz, J. (2011). The reliability of [C II] as an indicator of the star formation rate. *Monthly Notices of the Royal Astronomical Society*, 416(4):2712–2724.

[de Ugarte Postigo, A. et al., 2012] de Ugarte Postigo, A., Lundgren, A., Martín, S., Garcia-Appadoo, D., de Gregorio Monsalvo, I., Peck, A., Michalowski, M. J., Thöne, C. C., Campana, S., Gorosabel, J., Tanvir, N. R., Wiersema, K., Castro-Tirado, A. J., Schulze, S., De Breuck, C., Petitpas, G., Hjorth, J., Jakobsson, P., Covino, S., Fynbo, J. P. U., Winters, J. M., Bremer, M., Levan, A. J., Llorente, A., Sánchez-Ramírez, R., Tello, J. C., and Salvaterra, R. (2012). Pre-alma observations of grbs in the mm/submm range. *A&A*, 538:A44.

[Dekel et al., 2009] Dekel, A., Birnboim, Y., Engel, G., Freundlich, J., Goerdt, T., Mumcuoglu, M., Neistein, E., Pichon, C., Teyssier, R., and Zinger, E. (2009). Cold streams in early massive hot haloes as the main mode of galaxy formation. *Nature*, 457:451 EP –.

[Eggen et al., 1962] Eggen, O. J., Lynden-Bell, D., and Sandage, A. R. (1962). Evidence from the motions of old stars that the Galaxy collapsed. *The Astrophysical Journal*, 136:748.

[Fan et al., 2006] Fan, X., Strauss, M. A., Becker, R. H., White, R. L., Gunn, J. E., Knapp, G. R., Richards, G. T., Schneider, D. P., Brinkmann, J., and Fukugita, M. (2006). Constraining the evolution of the ionizing background and the epoch of reionization with $z \sim 6$ quasars. II. a sample of 19 quasars. *The Astronomical Journal*, 132(1):117–136.

[Faucher-Giguère et al., 2013] Faucher-Giguère, C.-A., Quataert, E., and Hopkins, P. F. (2013). Feedback-regulated star formation in molecular clouds and galactic discs. *Monthly Notices of the Royal Astronomical Society*, 433(3):1970–1990.

[Fujimoto et al., 2019] Fujimoto, S., Ouchi, M., Ferrara, A., Pallottini, A., Ivison, R. J., Behrens, C., and Gallerani, S. (2019). First identification of 10-kpc scale [cii] 158μm halos around star-forming galaxies at z=5-7.

[Gill et al., 2004] Gill, S. P. D., Knebe, A., and Gibson, B. K. (2004). The evolution of substructure — I. A new identification method. *Monthly Notices of the Royal Astronomical Society*, 351(2):399–409.

[Hahn and Abel, 2011] Hahn, O. and Abel, T. (2011). Multi-scale initial conditions for cosmological simulations. *Monthly Notices of the Royal Astronomical Society*, 415(3):2101–2121.

[Hopkins, 2015] Hopkins, P. F. (2015). A new class of accurate, mesh-free hydrodynamic simulation methods. *Monthly Notices of the Royal Astronomical Society*, 450(1):53–110.

[Hopkins et al., 2014] Hopkins, P. F., Faucher-Giguère, C.-A., Kereš, D., Quataert, E., Bullock, J. S., Oñorbe, J., and Murray, N. (2014). Galaxies on FIRE (Feedback In Realistic Environments): stellar feedback explains cosmologically inefficient star formation. *Monthly Notices of the Royal Astronomical Society*, 445(1):581–603.

[Hopkins et al., 2005] Hopkins, P. F., Hernquist, L., Martini, P., Cox, T. J., Robertson, B., Matteo, T. D., and Springel, V. (2005). A physical model for the origin of quasar lifetimes. *The Astrophysical Journal*, 625(2):L71–L74.

[Hopkins et al., 2018a] Hopkins, P. F., Hummels, C., Wheeler, C., Schmitz, D., Escala, I., Su, K.-Y., Orr, M., Grudić, M. Y., Sanderson, R., Garrison-Kimmel, S., Ma, X., Wetzel, A., Torrey, P., Kim, J.-H., Bullock, J. S., Elbert, O. D., Narayanan, D., Kereš, D., Chan, T. K., Faucher-Giguère, C.-A., Anglés-Alcázar, D., Hafen, Z., Quataert, E., Feldmann, R., Fitts, A., Boylan-Kolchin, M., Murray, N., and Hayward, C. C. (2018a). FIRE-2 simulations: physics versus numerics in galaxy formation. *Monthly Notices of the Royal Astronomical Society*, 480(1):800–863.

[Hopkins et al., 2018b] Hopkins, P. F., Orr, M. E., Hayward, C. C., Kereš, D., Chan, T. K., Faucher-Giguère, C.-A., Feldmann, R., Quataert, E., and Murray, N. (2018b). What FIREs up star formation: the emergence of the Kennicutt–Schmidt law from feedback. *Monthly Notices of the Royal Astronomical Society*, 478(3):3653–3673.

[Hopkins et al., 2012] Hopkins, P. F., Quataert, E., and Murray, N. (2012). The structure of the interstellar medium of star-forming galaxies. *Monthly Notices of the Royal Astronomical Society*, 421(4):3488–3521.

[Katz, 1992] Katz, N. (1992). Dissipational galaxy formation. II - effects of star formation. *Astrophysical Journal*, 391(2):502–517.

[Kim et al., 2011] Kim, C.-G., Kim, W.-T., and Ostriker, E. C. (2011). Regulation of star formation rates in multiphase galactic disks: Numerical tests of the thermal/dynamical equilibrium model. *The Astrophysical Journal*, 743(1):25–52.

[Knollmann and Knebe, 2009] Knollmann, S. R. and Knebe, A. (2009). AHF: AMIGA's halo finder. *The Astrophysical Journal Supplement Series*, 182(2):608–624.

[Knudsen et al., 2016] Knudsen, K. K., Richard, J., Kneib, J.-P., Jauzac, M., Clément, B., Drouart, G., Egami, E., and Lindroos, L. (2016). [C ii] emission in z ∼6 strongly lensed, star-forming galaxies. *Monthly Notices of the Royal Astronomical Society: Letters*, 462(1):L6–L10.

[Kohandel et al., 2019] Kohandel, M., Pallottini, A., Ferrara, A., Zanella, A., Behrens, C., Carniani, S., Gallerani, S., and Vallini, L. (2019). Kinematics of $z \geq 6$ galaxies from [CII] line emission.

[Kovetz et al., 2017] Kovetz, E. D., Viero, M. P., Lidz, A., Newburgh, L., Rahman, M., Switzer, E., Kamionkowski, M., Aguirre, J., Alvarez, M., Bock, J., Bond, J. R., Bower, G., Bradford, C. M., Breysse, P. C., Bull, P., Chang, T.-C., Cheng, Y.-T., Chung, D., Cleary, K., Corray, A., Crites, A., Croft, R., Doré, O., Eastwood, M., Ferrara, A., Fonseca, J., Jacobs, D., Keating, G. K., Lagache, G., Lakhlani, G., Liu, A., Moodley, K., Murray, N., Pénin, A., Popping, G., Pullen, A., Reichers, D., Saito, S., Saliwanchik, B., Santos, M., Somerville, R., Stacey, G., Stein, G., Villaescusa-Navarro, F., Visbal, E., Weltman, A., Wolz, L., and Zemcov, M. (2017). Line-intensity mapping: 2017 status report.

[Lagache et al., 2018] Lagache, G., Cousin, M., and Chatzikos, M. (2018). Vizier online data catalog: [cii] luminosities of galaxies in g.a.s.+cloudy. *A&A*, 609:A130.

[Lucy, 1999] Lucy, L. B. (1999). Computing radiative equilibria with monte carlo techniques. *A&A*, 344:282–288.

[Lupi and Bovino, 2019] Lupi, A. and Bovino, S. (2019). The [cii]–sfr correlation in dwarf galaxies across cosmic time.

[Ma et al., 2018a] Ma, X., Hopkins, P. F., Boylan-Kolchin, M., Faucher-Giguère, C.-A., Quataert, E., Feldmann, R., Garrison-Kimmel, S., Hayward, C. C., Kereš, D., and Wetzel, A. (2018a). Simulating galaxies in the reionization era with FIRE-2: morphologies and sizes. *Monthly Notices of the Royal Astronomical Society*, 477(1):219–229.

[Ma et al., 2018b] Ma, X., Hopkins, P. F., Garrison-Kimmel, S., Faucher-Giguère, C.-A., Quataert, E., Boylan-Kolchin, M., Hayward, C. C., Feldmann, R., and Kereš, D. (2018b). Simulating galaxies in the reionization era with FIRE-2: galaxy scaling relations, stellar mass functions, and luminosity functions. *Monthly Notices of the Royal Astronomical Society*, 478(2):1694–1715.

[Maiolino et al., 2015] Maiolino, R., Carniani, S., Fontana, A., Vallini, L., Pentericci, L., Ferrara, A., Vanzella, E., Grazian, A., Gallerani, S., Castellano, M., Cristiani, S., Brammer, G., Santini, P., Wagg, J., and Williams, R. (2015). The assembly of 'normal' galaxies at z $\sim$ 7 probed by ALMA. *Monthly Notices of the Royal Astronomical Society*, 452(1):54–68.

[Matthee et al., 2015] Matthee, J., Sobral, D., Santos, S., Röttgering, H., Darvish, B., and Mobasher, B. (2015). Identification of the brightest Lyα emitters at z = 6.6: implications for the evolution of the luminosity function in the reionization era. *Monthly Notices of the Royal Astronomical Society*, 451(1):400–417.

[McGreer et al., 2011] McGreer, I. D., Mesinger, A., and Fan, X. (2011). The first (nearly) model-independent constraint on the neutral hydrogen fraction at z $\sim$ 5–6. *Monthly Notices of the Royal Astronomical Society*, 415(4):3237–3246.

[Moster et al., 2012] Moster, B. P., Naab, T., and White, S. D. M. (2012). Galactic star formation and accretion histories from matching galaxies to dark matter haloes . *Monthly Notices of the Royal Astronomical Society*, 428(4):3121–3138.

[Ota et al., 2014] Ota, K., Walter, F., Ohta, K., Hatsukade, B., Carilli, C. L., da Cunha, E., González-López, J., Decarli, R., Hodge, J. A., Nagai, H., Egami, E., Jiang, L., Iye, M., Kashikawa, N., Riechers, D. A., Bertoldi, F., Cox, P., Neri, R., and Weiss, A. (2014). ALMA observation of 158 μm [C II] line and dust continuum of a $z = 7$ normally star-forming galaxy in the epoch of reionization. *The Astrophysical Journal*, 792(1):34.

[Ouchi et al., 2013] Ouchi, M., Ellis, R., Ono, Y., Nakanishi, K., Kohno, K., Momose, R., Kurono, Y., Ashby, M. L. N., Shimasaku, K., Willner, S. P., Fazio, G. G., Tamura, Y., and Iono, D. (2013). An intensely star-forming galaxy at $z \sim 7$ with low dust and metal content revealed by deep ALMA and HST observations. *The Astrophysical Journal*, 778(2):102.

[Ouchi et al., 2009] Ouchi, M., Mobasher, B., Shimasaku, K., Ferguson, H. C., Fall, S. M., Ono, Y., Kashikawa, N., Morokuma, T., Nakajima, K., Okamura, S., Dickinson, M., Giavalisco, M., and Ohta, K. (2009). Large area survey for $z = 7$ galaxies in SDF and GOODS-N: implications for galaxy formation and cosmic reionisation. *The Astrophysical Journal*, 706(2):1136–1151.

[Pallottini et al., 2017] Pallottini, A., Ferrara, A., Bovino, S., Vallini, L., Gallerani, S., Maiolino, R., and Salvadori, S. (2017). The impact of chemistry on the structure of high-z galaxies. *Monthly Notices of the Royal Astronomical Society*, 471(4):4128–4143.

[Pallottini et al., 2016] Pallottini, A., Ferrara, A., Gallerani, S., Vallini, L., Maiolino, R., and Salvadori, S. (2016). Zooming on the internal structure of z $\simeq$ 6 galaxies. *Monthly Notices of the Royal Astronomical Society*, 465(3):2540–2558.

[Pascucci et al., 2004] Pascucci, I., Wolf, S., Steinacker, J., Dullemond, C. P., Henning, T., Niccolini, G., Woitke, P., and Lopez, B. (2004). The 2d continuum radiative transfer problem. *A&A*, 417(3):793–805.

[Pentericci et al., 2016] Pentericci, L., Carniani, S., Castellano, M., Fontana, A., Maiolino, R., Guaita, L., Vanzella, E., Grazian, A., Santini, P., Yan, H., Cristiani, S., Conselice, C., Giavalisco, M., Hathi, N., and Koekemoer, A. (2016). Tracing the reionization epoch with ALMA: [C II] emission in $z \sim 7$ galaxies. *The Astrophysical Journal*, 829(1):L11.

[Planck Collaboration, 2016] Planck Collaboration (2016). Planck 2015 results - xiii. cosmological parameters. *A&A*, 594:A13.

[Quataert et al., 2011] Quataert, E., Hopkins, P. F., and Murray, N. (2011). Self-regulated star formation in galaxies via momentum input from massive stars. *Monthly Notices of the Royal Astronomical Society*, 417(2):950–973.

[Richings et al., 2014a] Richings, A. J., Schaye, J., and Oppenheimer, B. D. (2014a). Non-equilibrium chemistry and cooling in the diffuse interstellar medium – I. Optically thin regime. *Monthly Notices of the Royal Astronomical Society*, 440(4):3349–3369.

[Richings et al., 2014b] Richings, A. J., Schaye, J., and Oppenheimer, B. D. (2014b). Non-equilibrium chemistry and cooling in the diffuse interstellar medium – II. Shielded gas. *Monthly Notices of the Royal Astronomical Society*, 442(3):2780–2796.

[Shetty and Ostriker, 2008] Shetty, R. and Ostriker, E. C. (2008). Cloud and Star Formation in Disk Galaxy Models with Feedback. *The Astrophysical Journal*, 684(2):978–995.

[Smit et al., 2018] Smit, R., Bouwens, R. J., Carniani, S., Oesch, P. A., Labbé, I., Illingworth, G. D., van der Werf, P., Bradley, L. D., Gonzalez, V., Hodge, J. A., Holwerda, B. W., Maiolino, R., and Zheng, W. (2018). Rotation in [C II]-emitting gas in two galaxies at a redshift of 6.8. *Nature*, 553:178 EP –.

[Sobolev, 1957] Sobolev, V. V. (1957). The diffusion of L_α-radiation in nebulae and stellar envelopes. *Soviet Astronomy*, 1:678.

[Toomre, 1964] Toomre, A. (1964). On the gravitational stability of a disk of stars. *The Astrophysical Journal*, 139:1217–1238.

[White and Rees, 1978] White, S. D. M. and Rees, M. J. (1978). Core condensation in heavy halos: a two-stage theory for galaxy formation and clustering. *Monthly Notices of the Royal Astronomical Society*, 183(3):341–358.

Acknowledgements

I would like to thank Norman MURRAY for having me at CITA for five months providing me hindsight on a field on which I did not know much at the beginning of the internship, as well as for the time he regularly spent to follow up the progress of my work. I am thankful to him for helping me with all the visa and administrative issues.
I would like to thank Laura KEATING for her constant help and support all along the five months and her very helpful feedback on my work. I was happy that she was able to guide me through the programmes I had to use, be it GIZMO, CHIMES,RADMC-3D, AHF or astrophysics python modules.
I would like to thank CJ WOODFORD for organising the RANDOAstro group meeting every Thursday of my stay and giving the opportunity to present my work at the end of my stay to the whole Norm Murray Group.
I would like to thank the whole group for the presentations they gave on a lot of astrophysics topics I did not know and for their feedback on my work.
Finally I would like to thank the complete CITA team, Jenny JUNG, Candace DUONG, and all the others for their warm welcome during the coldest part of the year in Toronto.

Astrophysics and cosmology conventions

Atoms and ions names

In astrophysics there is a writing convention for the emission line of the atoms and atomic ions. We use those names to refer to the lines rather than the usual chemical names of the atom of ion. The rule is simple, for an atom A, the neutral atom line will be written AI with a roman number. The positive ions lines will be written as follows: $A^+ \to A$II, $A^{2+} \to A$III, $A^{3+} \to A$IV, and so on...
The line corresponding to the deexcitation of $A^{\mathrm{n}+}$ will be written A followed by $n+1$ in roman number. The roman number can also be written in lower index and the ion name can also be between square brackets. Here I will do both to better highlight the line.
For example, in this report I wrote the line corresponding to the mechanical deexcitation of C^+ as $[\mathrm{C_{II}}]$[1].

Units

In theoretical astrophysics one has to use the same units that the observers do in order to be able to easily compare both theoretical results and observational data. If most usually used units make sense because of their scale, some are just remnants of traditional observations methods. The units also depend on the sub-field of astrophysics at hand. For example when one studies planetary dynamics or proto-planetary disk the usual length unit is the astronomical unit (au), but for the study of larger structures like galaxies, it comes in handier to use parsecs (pc). The "default" units are the ones of the CGS (centimetre-gram-second) system rather than the nowadays more common international system of units (metre-kilogram-second). Below is non-exhaustive list of the most used units throughout this report and how they compare to one another. From now on the units will always be specified as their choice is not obvious.

Dimension	**Unit symbols**	**Unit description**
Mass	g or $\mathrm{M}_\odot$	gram or solar mass (1 $\mathrm{M}_\odot$= 1.98847 $\times 10^{33}$g)
Length	cm or pc	centimetre or parsec (1 pc = 3.0857 $\times 10^{18}$ cm)
Time	s or y	second or year (1 y $\simeq \pi \times 10^7$ s)
Energy	erg	Erg, the CGS unit of energy.
Spectral flux density	erg s^{-1} cm^{-2} Hz^{-1} or Jy	CGS unit or jansky (1 Jy = 10^{-23} erg s^{-1} cm^{-2} Hz^{-1})

Table 1: Table of usual astrophysics units used in this report.

Constants

Symbol	**Description**	**Value (usual units)**
h	The reduced Hubble ratio – the expansion rate	~ 0.7 (dimensionless)

The use of h in cosmological simulations comes from when the value of Hubble's constant was very uncertain. More detailed explanations can be found in [Croton, 2013].

[1]For C^+ it is very convenient and non-ambiguous as there only is one line.